The deflection of reinforced concrete beams containing recycled steel fibers

Received: 13 November 2020 | Revised: 3 March 2021 | Accepted: 10 April 2021

DOI: 10.1002/suco.202000729

TECHNICAL PAPER

fib CEB-FIP WILEY

The deflection of reinforced concrete beams containing recycled steel fibers

Alessandro P. Fantilli[1] | **Benedetta Orfeo**[2] | **Alejandro Pérez Caldentey**[3]

[1]Department of Structural, Building and Geotechnical Engineering, Politecnico di Torino, Torino, Italy

[2]Department of Continuum Mechanics and Structures, Universidad Politécnica de Madrid, Madrid, Spain

[3]Department of Mechanics of Continuous Media and Theory of Structures, Technical University of Madrid & FHECOR Consulting Engineers, Madrid, Spain

Correspondence
Alessandro P. Fantilli, Department of Structural, Building and Geotechnical Engineering, Politecnico di Torino, Corso Duca degli Abruzzi 24, 10129 Torino, Italy.
Email: alessandro.fantilli@polito.it

Funding information
Centro de Desarrollo Tecnológico Industrial, Grant/Award Number: IDI-20110480

Abstract

A 3-stage model is used to evaluate the results of an experimental campaign, previously carried out with the aim of studying the deflection of reinforced concrete structures made with reinforced concrete (RC) and fiber-reinforced concrete (R/FRC). In particular, 12 four-point bending tests were performed on beams, whose cross-sections were obtained by combining four effective ratios of the tensile reinforcement (i.e., 0.73%, 1.7%, 3%, and 6.3%), two concrete covers (i.e., 32 mm and 82 mm), and three amounts of steel fibers (0, 0.5%, and 1.0% in volume) recycled from end-of-life tyres. In reinforced beams with low reinforcement ratios, there is a reduction in deflections and the load at yielding of steel increases with the content of fibers. On the contrary, the mechanical behavior of R/FRC and RC beams does not substantially differ in presence of a high effective reinforcement ratio. These experimental observations are in accordance with the results of the three-stage model, introduced herein to predict the possible variation of the load-deflection curves. For a given deflection, the model provides a possible range of applied loads, whose upper bound is related to the situation of incipient cracking (i.e., the maximum tension stiffening effects), whereas the lower bound concerns a fully cracked beam (i.e., the minimum tension stiffening effects). Regardless of the content of fibers, the difference between the upper and lower bounds vanishes in highly reinforced concrete beams.

KEYWORDS

four-point bending tests, FRC, load-deflection diagrams, moment-curvature relationship, tension-stiffening, three-stage model

1 | INTRODUCTION

In the last years, deflection control of reinforced concrete (RC) elements has become more important. Indeed, the limits of deformation are the most critical requirement, especially in beams subject to bending actions.[1] In

Discussion on this paper must be submitted within two months of the print publication. The discussion will then be published in print, along with the authors' closure, if any, approximately nine months after the print publication.

designing new constructions, the depth of RC beams can be determined by slenderness limits which, for a given span, provide a minimum effective depth.[2,3] These limits provide enough stiffness and to avoid total deflections larger than 1/250 of the span length and deflection happening after the construction of partitions larger than 1/500 of the span. The latter is normally the appropriate limit for quasi-permanent loads when deflections can damage adjacent structural or non-structural components.[4]

In the serviceability stage, deflection depends on the stiffness of RC beams, which is in turn reduced by the presence of cracks in the tensile zones. As cracking is a random phenomenon, the so-called tension-stiffening effect (i.e., the stiffness of concrete in tension between two consecutive cracks) varies within a range.[5] The amplitude of this range depends on the percentage of reinforcement in the tensile zone, on the concrete cover and on the presence of fibers in the cement-based matrix.[6]

In fiber-reinforced concrete (FRC), the bridging effect of fibers tends to reduce the crack width.[7] Thus, in R/FRC beams, reinforced by both rebar and fibers (so-called hybrid reinforcement), the limitation of crack width is easier to satisfy than in RC beams under the same service loads.[8] Also, the stiffness of FRC structures is expected to be greater than that of plain concrete structures.[9] Nevertheless, deflections in R/FRC beams are not always lower than those of RC beams, as recently shown by Hamrat et al..[10] Indeed, the influence of steel fibers in increasing the stiffness of cracked cross-sections depends on the amount of longitudinal rebar in tension.[11] Moreover, models used to calculate the deflection of RC beams, and based on the definition of a single moment-curvature (M–χ) relationship,[12] are not always effective in computing the deformation of R/FRC beams. Indeed, the possible variations of tension-stiffening caused by the randomness of crack patterns, and by the presence of fibers, are generally not included in the calculation of M–χ diagram.

Thus, a new range model for M–χ, similar to that used to predict the behavior of reinforced concrete ties,[6] is also desirable for R/FRC beams. Through this model, the capacity of Recycled Steel Fibers (RSF) to improve the mechanical and environmental performance of concrete beams can be definitely assessed.[13] The investigations on reinforced concrete beams containing recycled steel fibers are very scarce, especially in the serviceability stage. Thus, the results of the experimental and theoretical analyses presented herein, can contribute to the design of R/FRC beams containing RSF and to reduce the environmental impact of the construction industry as well.

2 | DESCRIPTION OF THE EXPERIMENTAL INVESTIGATION

The results of the tests performed on 12 full-scale beams at the Technical University of Madrid (UPM),[14–17] are described and analyzed in the following sections.

2.1 | Materials

Eight of the beams have been cast with Self-Compacting Concrete (SCC) containing RSF from end-of-life tyres. The composition of SCC is shown in the Table 1. RSF, which are generally crooked after the shredding process, have variable length and aspect ratio (average length = 15 mm, and average aspect ratio = 100). Two cement-based mixtures, B and C, made with the same SCC, but containing different percentage in volume of RSF (i.e., 0.5%, and 1%, respectively), have been compared with a previous experimental campaign. In this campaign, four beams with the same geometry but cast using conventional RC (mix type A) were tested.[16] The mechanical properties of these concretes are listed in Table 2. In particular, the average value of the compressive strength, f_{cm}, has been measured by means of uniaxial compression tests cylinders (diameter = 150 mm, and height 300 mm). In the case of FRC (i.e., only in concretes B and C), in accordance with EN 14621,[17] notched prismatic specimens $150 \times 150 \times 600$ mm have been tested in three-point bending to measure the Limit of Proportionality (LOP), and the residual strengths f_{R1}, f_{R2}, f_{R3} and f_{R4}. Finally, B-500 C steel reinforcing bars have been used to reinforce all the beams.

2.2 | Specimens and test setup

Figure 1a shows the configuration of the statically determinate beams tested in four-point bending. The beams have the same rectangular cross-sections (width = 350 mm, and depth = 450 mm) and reinforcement (four reinforcing bars in tension, two in the middle, and two in the compression

TABLE 1 Self-compacting concrete used to cast RC and R/FRC beams

CEM II AM (P–V)	400 kg/m^3
Water	165 kg/m^3
Aggregate 0/5 mm	1004 kg/m^3
Aggregate 5/10 mm	821 kg/m^3
Superplasticizer	3.7 L/m^3

TABLE 2 Mechanical properties of plain concrete and FRC

Type of concrete	f_c (MPa)	LOP (MPa)	f_{R1} (MPa)	f_{R2} (MPa)	f_{R3} (MPa)	f_{R4} (MPa)
A	26.9	—	—	—	—	—
B	36.4	3.10	1.53	1.08	0.51	0
C	37.5	3.53	2.21	1.72	1.26	0.725

zone). Nevertheless, the diameter of reinforcement and the size of concrete cover vary as follows:

- Beam 12-20 (Figure 1b), having a clear concrete cover $c = 20$ mm to the stirrup, 32 mm to the longitudinal bar and reinforced with 8 rebars with a diameter $\Phi = 12$ mm (2 in the compression zone, 2 in the middle, and 4 the tensile zone)
- Beam 12-70 (Figure 1c), reinforced as Beam 12-20 but with a clear concrete cover $c = 70$ mm to the stirrups, 82 mm to the longitudinal bars;
- Beam 25-20 (Figure 1d) reinforced by 4 rebars $\Phi = 25$ mm in the tensile zone and 4 rebars $\Phi = 12$ mm in the rest of the cross-section (2 in the compression and in the central part); the size of the concrete cover is $c = 20/32$ mm;
- Beam 25-70 (Figure 1e) reinforced as Beam 25-20 but with a concrete cover $c = 70/82$ mm.

As each type of beam has been made with the three concretes of Table 1, 4 series of 3 beams have been cast (see Table 3). By testing them in four-point bending, it has been possible to correlate the mechanical response of RC and R/FRC beams under flexure with the effect produced by the percentage of rebar in the tensile zone, the depth of concrete cover and by the fiber volume fraction. The beams have been labeled with the code *XX-YY-Z*, where *XX* = diameter in mm of rebar in tension (i.e., 12 mm or 25 mm); *YY* = depth of concrete cover to the stirrup (i.e., 20 mm or 70 mm); and *Z* = type of concrete (i.e., A, B, or C).

In the four cross-sections shown in Figure 1, the effective tension area, $A_{c,\text{eff}}$ is hatched. For the sake of the simplicity, $A_{c,\text{eff}}$ is assumed to be the area of a rectangle having a width of 350 mm and a depth = 2·(450 mm − d) (where d = effective depth of the cross-section[18]). The ratio $\rho_{\text{eff}} = A_s/A_{c,\text{eff}}$ (where A_s is the area of the rebar in tension) is considered as the geometrical percentage of rebar in the tensile zone. As shown in Table 3, ρ_{eff} varies from 0.73% (in series 12-70) to 6.3% (the beams of 25-20 series).

To prevent shear failure, the beams have been also reinforced with stirrups (diameter = 12 mm and spacing =100 mm) in the cantilever regions.

In the four-point bending tests, loads are applied in the cantilever edges through a loading machine equipped with a loading cell of 500 kN. Each test has been performed by controlling the applied load P, which was increased in pre-established steps. LVDTs (having a base of 200 mm) have been used to measure the beam deflection as P increases (see Figure 1).

2.3 | Experimental results

As a result of the four-point bending tests, Figure 2 illustrates the load P (applied at the end of the cantilever parts) versus deflection η curves in the midspan of the constant moment zone. All the curves experimentally measured are limited to the deflection $\eta = 30$ mm, which corresponds to the end of the serviceability stage. Indeed, at this deflection, the yielding of steel rebar in tension has already occurred in all the beams.

Obviously, the higher the reinforcement ratio, the larger the bearing capacity of both RC and R/FRC beams. When $\eta = 30$ mm, the corresponding value of P varies between 170 and 210 kN in series 12-20 (Figure 2a) and series 12-70 (Figure 2b), whereas P is within the range 400–600 kN in series 25-20 (Figure 2c) and 25-70 (Figure 2d). Nevertheless, for the same type of cross-section and at the same deflection, R/FRC beams are generally stronger than RC beams.

In the serviceability stage (i.e., when $\eta < 30$ mm), when the area of rebar in tension is relatively small (i.e., series 12-20 in Figure 2a and 12-70 in Figure 2b), the deflections of RC beams tend to be larger than those of R/FRC for the same values of the applied load. On the contrary, highly reinforced concrete beams (i.e., series 25-20 in Figure 2c and 25-70 in Figure 2d) show an opposite tendency and deflections are larger in R/FRC beams.

To better analyze this behavior, also observed by Hamrat et al.,[10] it is possible to evaluate, for a given deflection η, the difference (in percent) between load measured in fiber-reinforced concrete beams and that of reinforced concrete beams:

$$\Delta p = \frac{P_{\text{R/FRC}} - P_{\text{RC}}}{P_{\text{RC}}} \cdot 100 \quad (1)$$

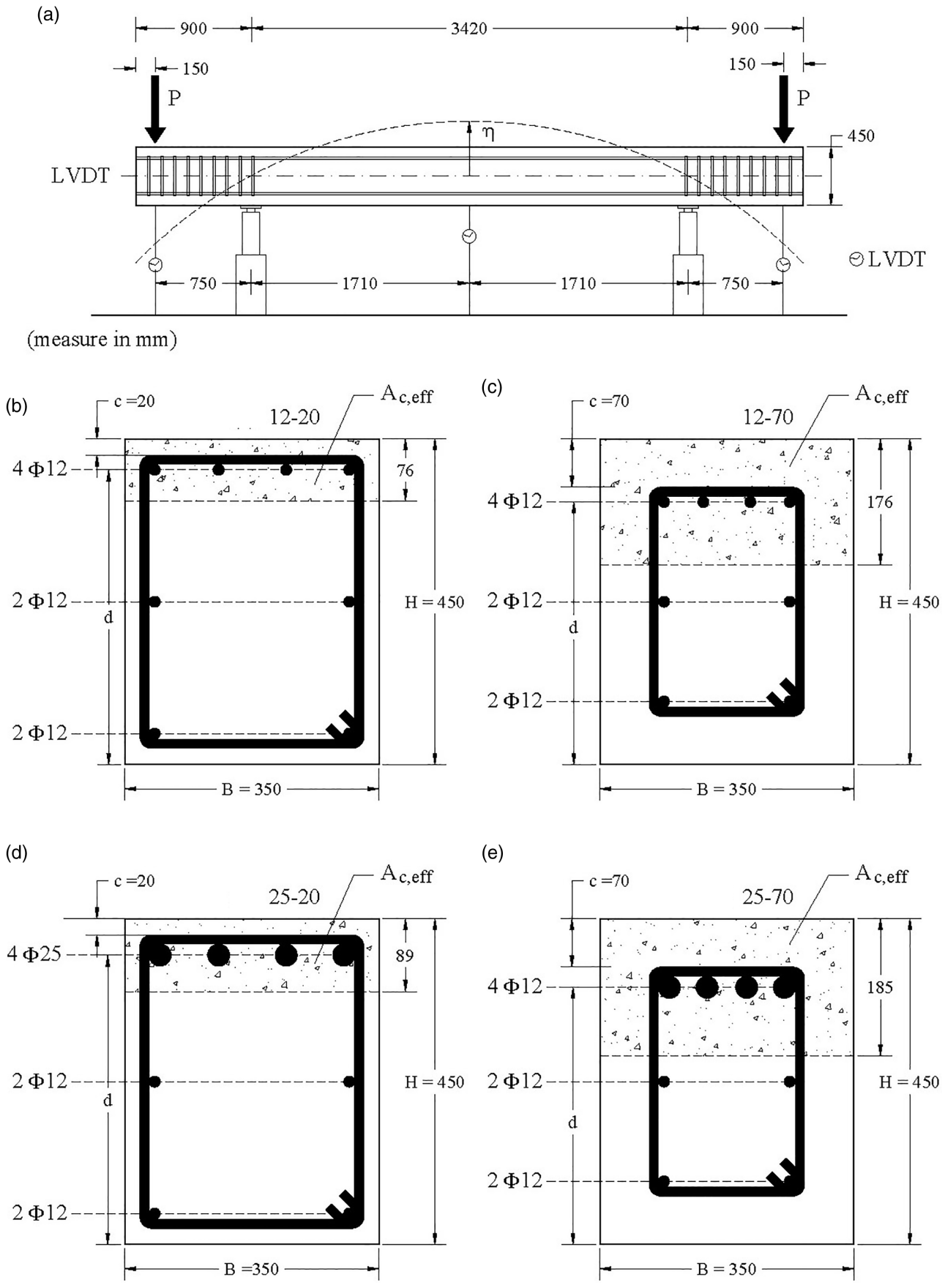

FIGURE 1 Four-point bending tests on RC and R/FRC beams: (a) geometrical properties and position of LVDT; (b)–(e) types of cross-section. All stirrups are 12 mm bars

TABLE 3 The beams investigated in the present research project

Type of cross-section	Specimen	Type of concrete	Concrete cover (mm)	Diameter of rebar in tension Φ (mm)	Effective percentage of rebar in tension ρ (%)
12-20 (Figure 1b)	12-20-A	A	20	12	1.7
	12-20-B	B			
	12-20-C	C			
12-70 (Figure 1c)	12-70-A	A	70	12	0.73
	12-70-B	B			
	12-70-C	C			
25-20 (Figure 1d)	25-20-A	A	20	25	6.3
	25-20-B	B			
	25-20-C	C			
25-70 (Figure 1e)	25-70-A	A	70	25	3.0
	25-70-B	B			
	25-70-C	C			

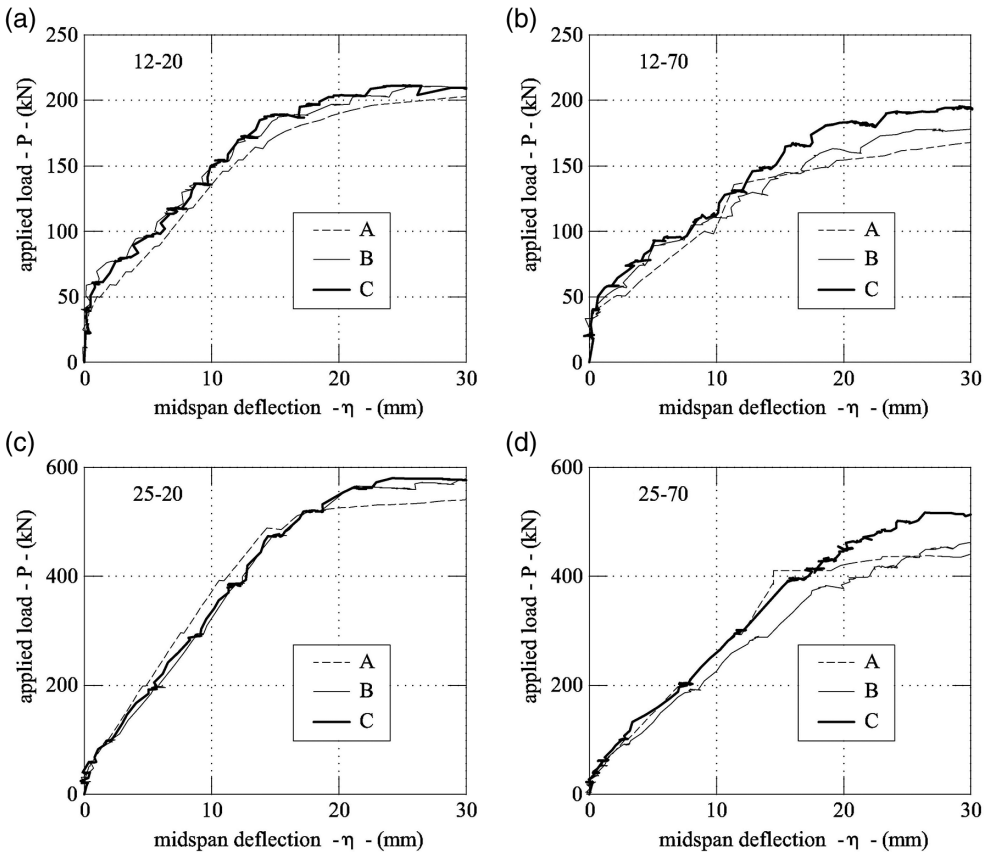

FIGURE 2 Load deflection curves measured in the experimental campaign: (a) cross-section 12-20; (b) cross-section 12-70 (c) cross-section 25-20; (d) cross-section 25-70

where, $P_{R/FRC}$ = load measured in the R/FRC beam at deflection η; P_{RC} = load measured in RC beam for the same deflection.

Figure 3a shows the values of Δp computed at $\eta = 7$ mm (which is 1/500 of the constant moment length in Figure 1a) in the R/FRC beams tested herein. These values depend on the type of FRC (i.e., B or C) and on the ratio ρ_{eff} of the reinforcement in tension with respect to the effective area. In particular, when the area of rebar is small, Δp is positive. Thus, in R/FRC beams, the deflection reaches the limit η = span length/500 when the load P is about 12% larger than that of RC beams. At the same deflection, if $\rho_{eff} > 2\%$, Δp becomes negative ($\cong -12\%$ in Figure 3a), and the load P is larger in RC than

in R/FRC beams. In other words, the experimental results reveal that fibers contribute to reduce the deflection of beams in bending when the effective percentage of reinforcement is lower than 2%. The bridging action of the fibers on the crack surfaces tends to reduce crack width and, contemporarily, the stiffness of the structure increases.[8]

When $\rho_{\text{eff}} > 2\%$, several narrow cracks interact with each other in the tensile zone of the concrete beams. Due to the growth of a new crack, the width of previously formed cracks is reduced, generating a state of compression. This phenomenon, which typically occurs in RC structures subjected to long-term cyclic actions,[19,20] generates a decrease in tension-stiffening and an increment in both curvatures and structural deflections. It was also observed in the first experimental analysis on the cracking of RC beams under monotonic loads.[21] Nevertheless, when rebar yields, the interaction between the cracks vanishes and in R/FRC beams the same deflections can be reached when loads are larger than those applied on RC beams. As Figure 3b shows, at $\eta = 30$ mm, the values of P increase with the percentage of reinforcement, and with the content of fibers as well.

Figure 4 provides a more detailed explanation of the decrease in tension-stiffening. When a new crack appears, the crack spacing is reduced and this leads to a reduction in the crack width. However, the mean steel strain is increased, and the mean concrete strain is reduced. Therefore, tension stiffening effects are reduced.

3 | THREE-STAGE MODEL FOR THE EVALUATION OF P–η

To predict the mechanical response of both RC and R/FRC beams, a range model, similar to that already developed for RC ties,[5] is proposed herein. In particular, for beams in four-point bending, the theoretical evaluation of the P–η curves is possible with a three-stage approach. First, to account for the maximum effect of tension-stiffening, an equivalent constitutive law of the steel rebar is evaluated. In the second stage, cross-sectional moment-curvature relationships are calculated both at incipient-cracking (i.e., with the maximum tension stiffening) and in fully cracked beams (i.e., without the contribution of tension-stiffening). Finally, the moment-curvature relationships are used to compute the theoretical range of P–η.

All the stages of the model are fully described in the following sections.

3.1 | Stage 1: Tension-stiffening model

According to the range model proposed by Fantilli et al.,[5] for a given load P, the deflection η of the beam depicted in Figure 1a varies. The range of variation depends on the tension-stiffening, which is in turn affected by the randomness of the crack pattern. All these phenomena are herein included within two constitutive laws for the steel rebar. The first law, which simulates the fully cracked beam, or the absence of tension-stiffening, coincides with the stress–strain (σ_s–ε_s) relationship of the naked rebar. On the contrary, to obtain the second relationship, a block of RC or R/FRC tie delimited by two consecutive cracks is analyzed (see Figure 5a). The block has a length s_r, which coincides with the crack spacing, and a cross-section corresponding to the tensile zone of the beams depicted in Figure 1b–e. Thus, in a single tie, $A_{c,\text{eff}}$ and A_s are the area of effective concrete and steel, respectively.

As the maximum effect of tension-stiffening has to be reproduced, the situation of incipient cracking is modeled through an equivalent σ_s–ε_s relationship of rebar. It corresponds to the onset of a new crack in the middle the tie (at $z = s_r/2$ in Figure 5a), and can be numerically

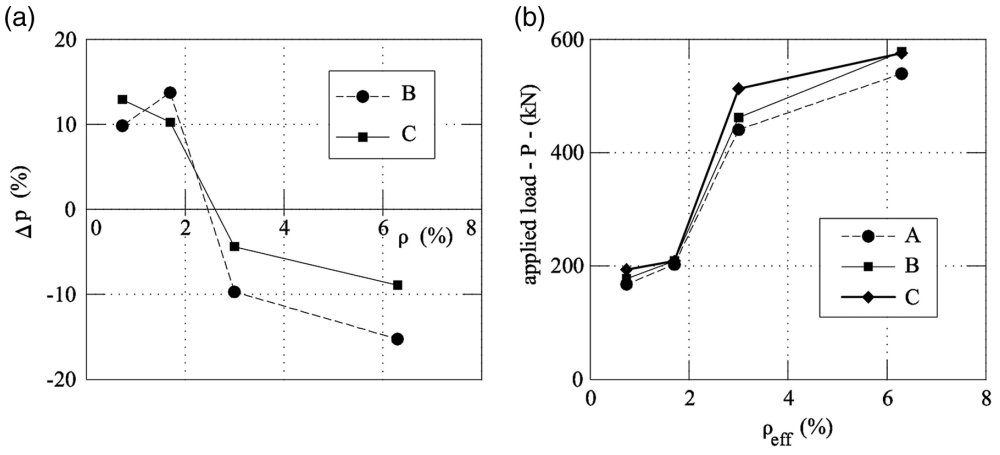

FIGURE 3 Results of the four-point bending tests on RC and R/FRC beams: (a) values of Δp in R/FRC beams as a function of the percentage ρ of rebar in tension; (b) the load P measured at $\eta = 30$ mm in all the beams

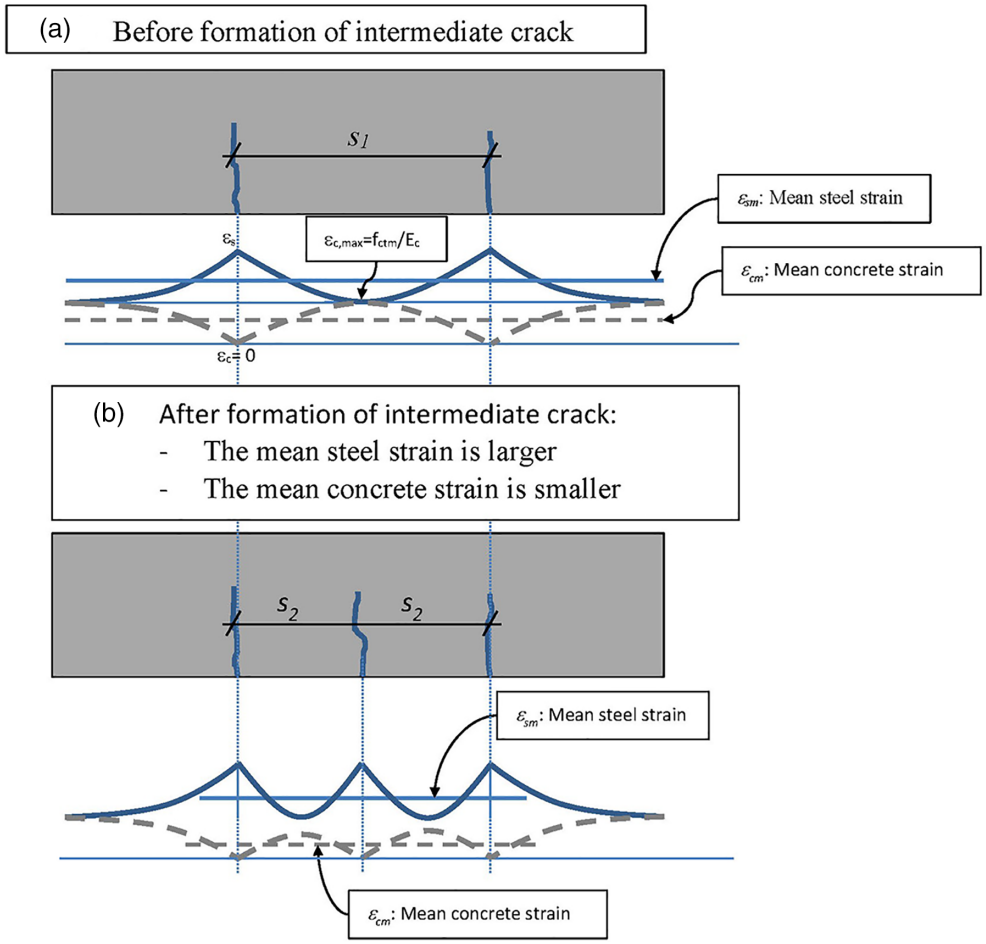

FIGURE 4 Explanation of how the formation of a new crack reduces the effects of tension-stiffening

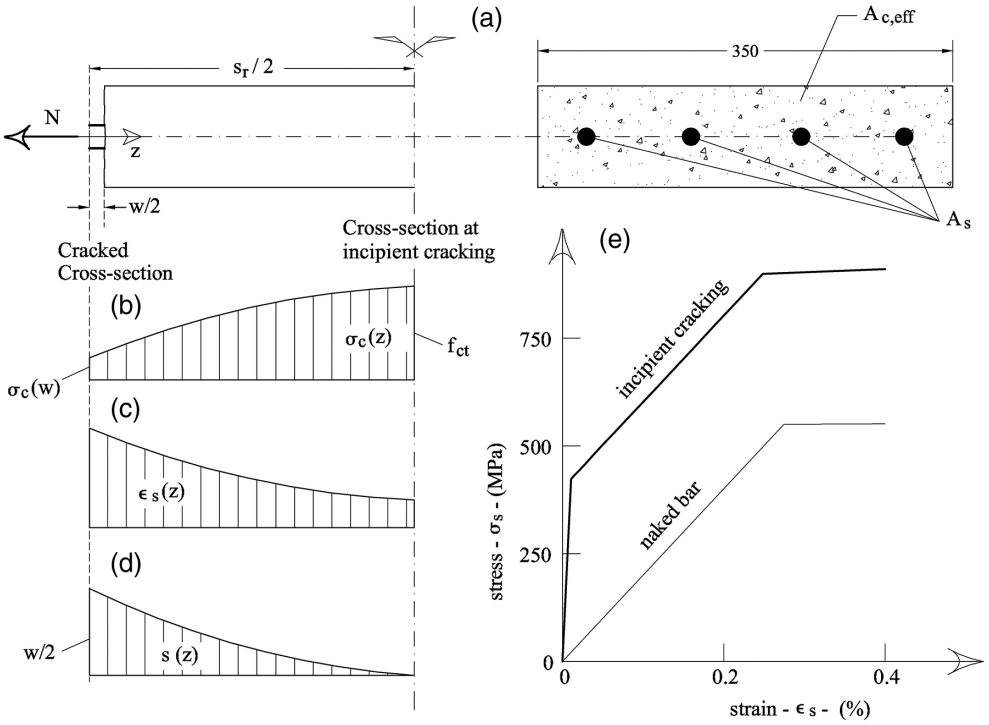

FIGURE 5 Evaluating the maximum effect of tension-stiffening in the three-stage model: (a) geometrical properties of the tie at incipient cracking: (b) distribution of tensile stress in concrete; (c) distribution of tensile strain in the reinforcement; (d) distribution of slip between steel and concrete; (e) stress–strain relationships of rebar in the beam 12-70-C

computed with the following procedure (Figure 5), which is repeated for different values of the crack width:

1. A value of crack width w is assumed in the cracked cross-section (Figure 5a);
2. A trial value is given to the strain in the reinforcement, ε_s, of the cracked cross-section (i.e., at $z = 0$);
3. To obtain the axial force N, the equilibrium equation can be written in the cracked cross-section:

$$N = \sigma_c(w)\, A_{c,\text{eff}} + \sigma_s(\varepsilon_s)\, A_s \tag{2}$$

where $\sigma_s(\varepsilon_s)$ = stress in the rebar computed, as a function of the strain ε_s, through the σ_s–ε_s relationship of the naked bar; and $\sigma_c(w)$ = stress in the cracked concrete. The latter is a function of crack width w (Figure 5b), according to the fictitious crack model of plain concrete[1] or FRC. The latter is in turn defined by means of the residual strength f_{R1} and f_{R4} of Table 2[6,17,22];

4. The equilibrium in the cross-section at incipient cracking, where the stress of concrete (or FRC) is $\sigma_c = f_{ct}$ (=tensile strength), provides the values of σ_s at $z = s_r/2$ (Figure 5a):

$$\sigma_s = (N - f_{ct} A_{c,\text{eff}})/A_s \tag{3}$$

The strain of the rebar in this cross-section, ε_s, is then computed with the stress–strain relationship of the naked bar;

5. A trial value for the distance between two cracks, s_r, is assumed;
6. As both the state of stress and strain are known at the borders of the tie depicted in Figure 1a, the following differential equations, which represents the equilibrium and compatibility conditions at the interface rebar—plain concrete or FRC (of the tension-stiffening problem[5]), can be numerically integrated (see also[22]):

$$\frac{d\sigma_s}{dz} = -\frac{p_s}{A_s}\tau \tag{4}$$

$$\frac{ds}{dz} = -\varepsilon_s(z) + \varepsilon_c(z) \tag{5}$$

where, p_s and A_s = perimeter and area of rebar, respectively; s = slip between steel and surrounding concrete (or FRC): z = horizontal coordinate; τ = bond stress on the interface rebar-plain concrete (or FRC). By considering the bond-slip, τ–s, relationship suggested by fib Model Code 2010,[1] the distribution of $\sigma_c(z)$ (in Figure 5b), $\varepsilon_s(z)$ (in Figure 5c), and $s(z)$ (in Figure 5d), respectively, within the domain $s_r/2$ are obtained.

7. If $s \neq 0$ in the cross-section at incipient cracking (i.e., at $z = s_r/2$ in Figure 5d), go back to step 6 with a new value of s_r;
8. If $\sigma_c \neq f_{ct}$ in the cross-section at incipient cracking (i.e., at $z = s_r/2$ in Figure 5b), go back to step 3 with a new value of ε_s in the cracked section (i.e., at $z = 0$ in Figure 5c).

For a given value of w, this procedure provides the corresponding normal force N applied to the ties of Figure 5a. The average strain of the rebar within the length s_r, calculated from the strain distribution $\varepsilon_s(z)$ as depicted in Figure 5c, corresponds to the strain of the σ_s–ε_s relationship at the incipient cracking (i.e., in condition of maximum tension-stiffening). For cross-section 12-70-C, Figure 5e shows the stress–strain relationship of the naked bar (which is that of steel B-500-C), corresponding to the fully cracked situation, and σ_s–ε_s of the incipient cracking obtained with the numerical procedure.

3.2 | Stage 2: Moment-curvature relationships

If the mechanical properties of rebar are known (both in the situations of incipient cracking and fully cracked behavior), cross-sectional moment-curvature (M–χ) relationships can be evaluated as follows (see Figure 6):

1. For a given value of the curvature χ (the normal force N is zero in this case),
2. Select a trial value for λ (which is the strain at the origin of the reference axis, that is, $y = 0$ in Figure 6a);
3. The state of strain is then computed assuming that plain sections remain plain after deformation (Figure 6b):

$$\varepsilon(y) = \lambda - \chi \cdot y \tag{6}$$

4. The state of stress $\sigma(y)$ of Figure 6c is computed from the stress–strain relationships of materials. In the case of incipient cracking, the constitutive relationship of rebar is given by the procedure described in the previous section. In the fully cracked situation, the σ_s–ε_s relationship of bare bar (Figure 5e) is used. In both the cases, the stress of concrete in tension is assumed

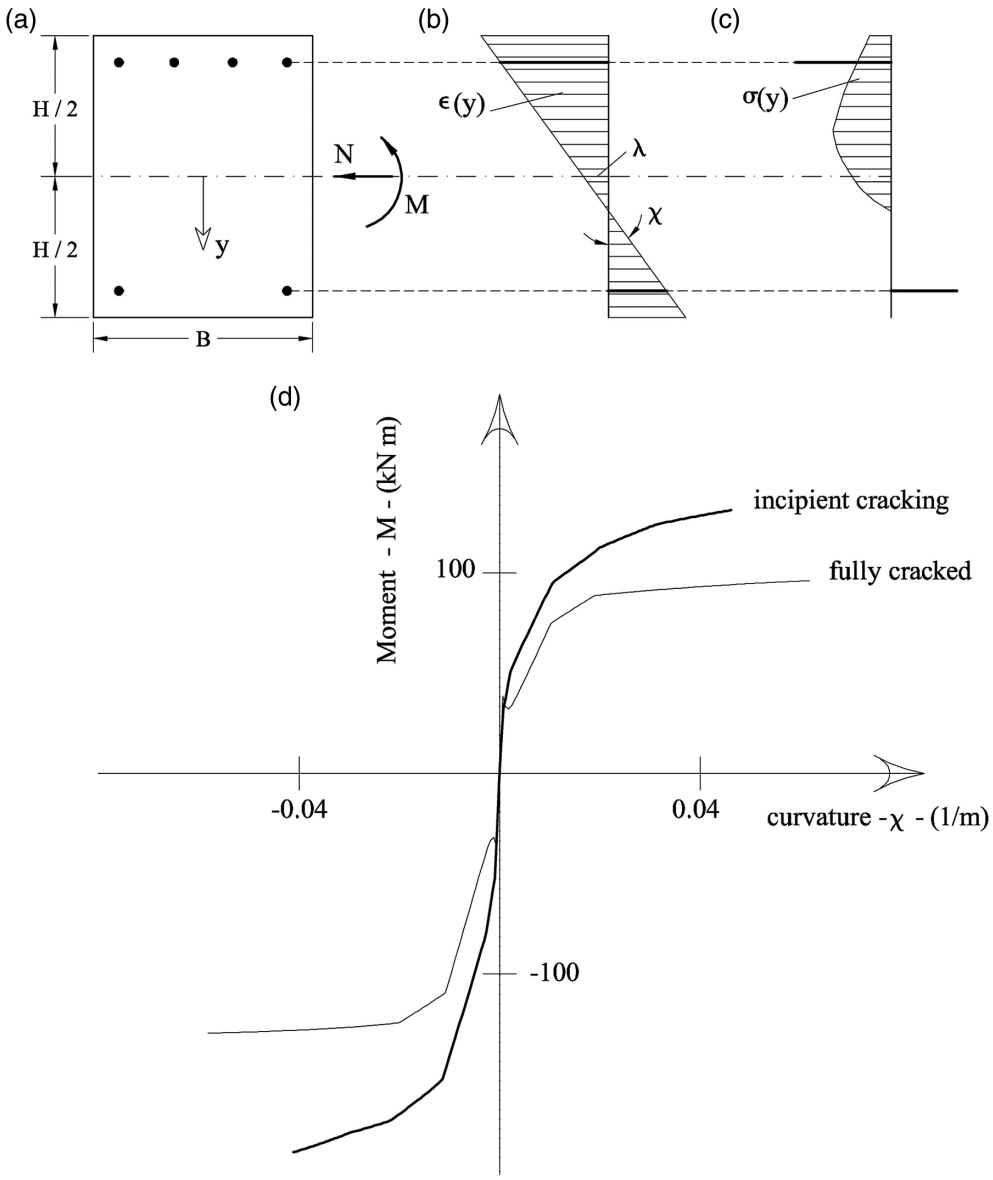

FIGURE 6 Evaluating the moment-curvature relationships: (a) geometrical properties of RC and R/FRC cross-sections; (b) linear strain profile in a cross-section; (c) the state of stress in a cross-section; (d) M–χ relationships computed for the beam 12-70-C

to be zero. Finally, Sargin's stress–strain relationship is used herein for concrete or FRC in compression.[1]

5. Compute the resultant of the state of stress N_R through the equilibrium equation:

$$N_R = B\int_{-\frac{H}{2}}^{\frac{H}{2}} \sigma(y)dy \tag{7}$$

where B = width of the cross-section; and H = height of the cross-section.

6. If $N_R \neq 0$, select a new value for λ and go back to step 3.
7. Compute the bending moment M with the following equation:

$$M = B\int_0^H \sigma(y)\cdot y\,dy \tag{8}$$

If this procedure is applied for all the possible values of χ, the whole moment-curvature relationship can be obtained. Figure 6d illustrates these relationships for the beams 12-70-C under the conditions of incipient cracking and fully cracked beam, respectively.

3.3 | Stage 3: Load-deflection diagram

When the geometry of the statically determinate beam depicted in Figure 1a is known, and the M–χ relationships of the cross-sections are both computed with the

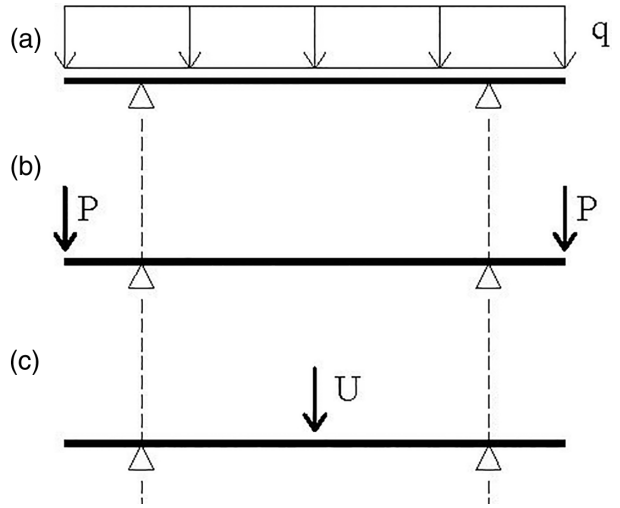

FIGURE 7 Evaluating of the load-deflection P–η diagram of a beam in bending: (a)–(b) loads acting on the real system; (c) load acting on the virtual system

previous procedures, the deflection η corresponding to an applied load P can be evaluated by (Figure 7):

1. Calculating in the real structure $M_b(z)$ the bending moment due to the application of the load P (Figure 7a) and of self-weight q (Figure 7b);
2. Using the moment–curvature relationship to calculate the distribution of the curvature $\chi_b(z)$ corresponding the moment $M_b(z)$;
3. Defining a virtual system (Figure 7c), made by the same beam and by a virtual load U, dual of the deflection η, to compute the bending moment $M_a(z)$;
4. Calculating the deflection η with the following equation (of virtual works):

$$\eta = \frac{1}{U}\int_0^L M_a(z)\cdot\chi_b(z)\,dz \tag{9}$$

where L is the length of the whole beam.

If these steps are repeated for all the values of P, the load-deflection curves, similar to those experimentally measured and reported in Figure 2, can be obtained.

For the sake of clarity, all the steps of the above-mentioned stages are summarized in the flow-chart depicted in Figure 8.

4 | COMPARISON BETWEEN THE EXPERIMENTAL DATA AND THE RESULTS OF THE MODEL

In the proposed three-stage model, the use of different types of concretes, plain or fiber-reinforced, is taken into

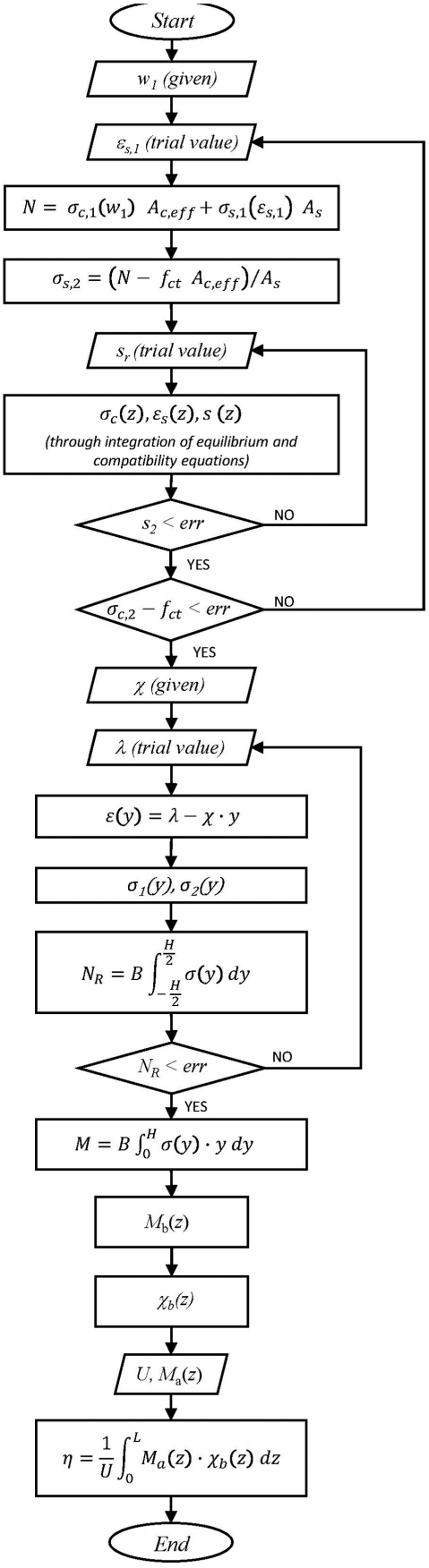

FIGURE 8 Flow-chart of the three-stage model

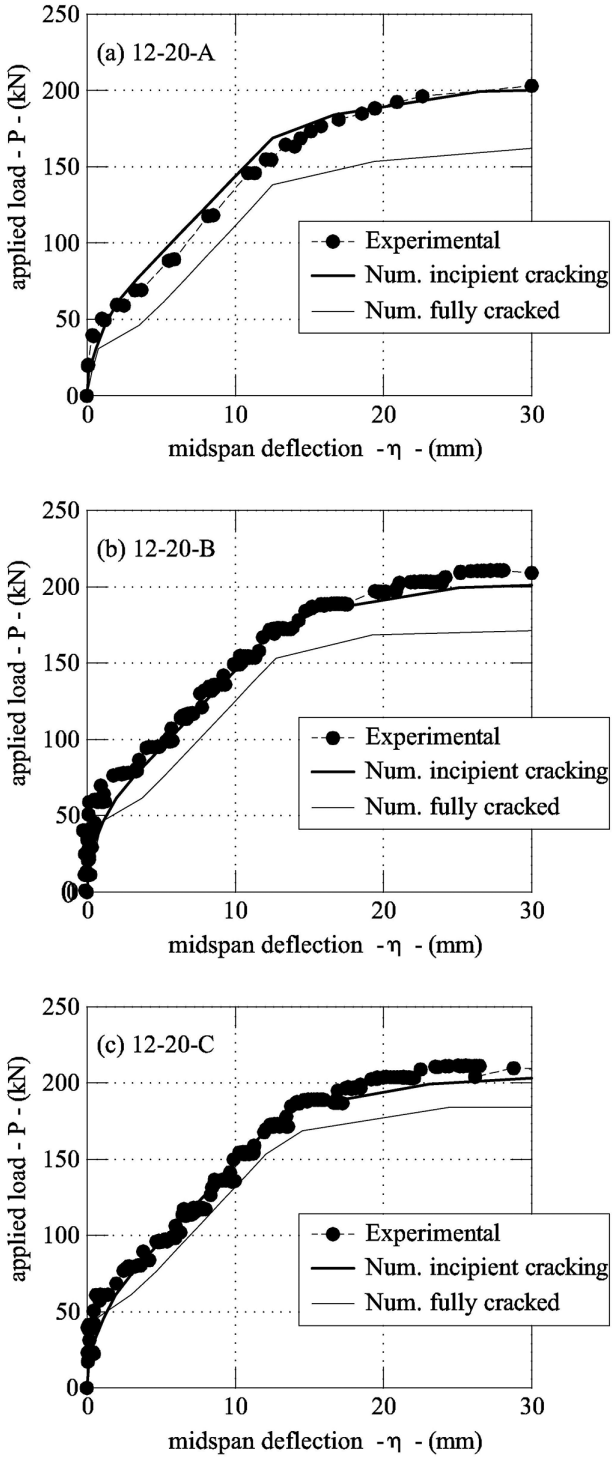

FIGURE 9 Comparison between the experimental data and the results of the three-stage model: (a) P–η curves of the beam 12-20-A; (b) P–η curves of the beam 12-20-B; (c) P–η curves of the beam 12-20-C

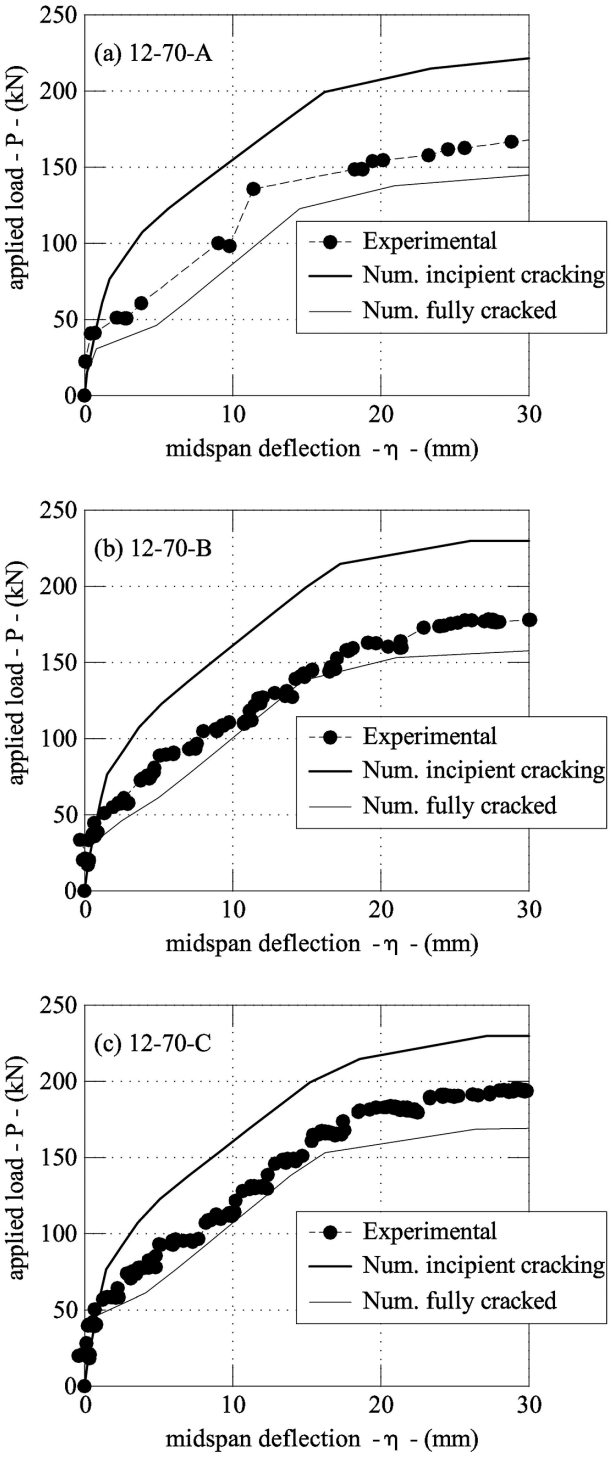

FIGURE 10 Comparison between the experimental data and the results of the three-stage model: (a) P–η curves of the beam 12-70-A; (b) P–η curves of the beam 12-70-B; (c) P–η curves of the beam 12-70-C

account within the constitutive relationships, which are defined according to the Model Code 2010.[1] In compression, when the fiber volume fraction is not high (as in this case), the mechanical response is not significantly affected by the presence of fibers (recycled or not). Therefore, the Sargin-type relationship has been used considering the mean strength reported in Table 2.

Regarding the concrete in tension, Model Code 2010[1] suggests modeling the material behavior of FRC only on the base of the post-cracking residual strengths, regardless of

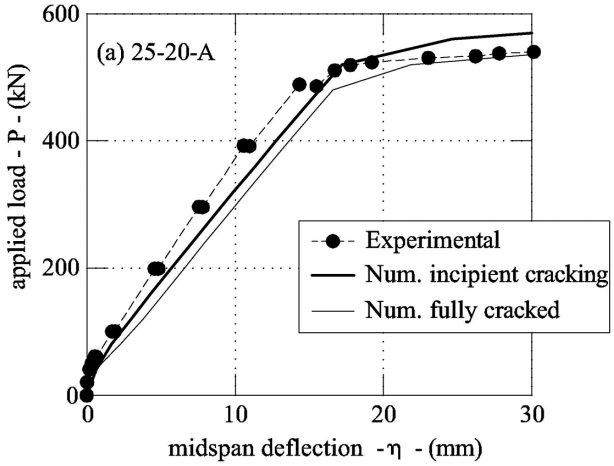

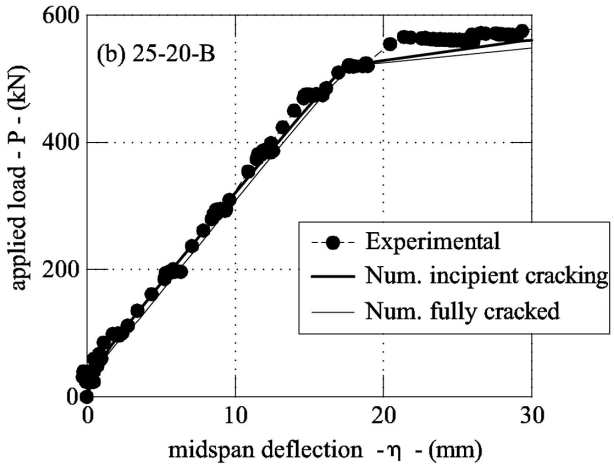

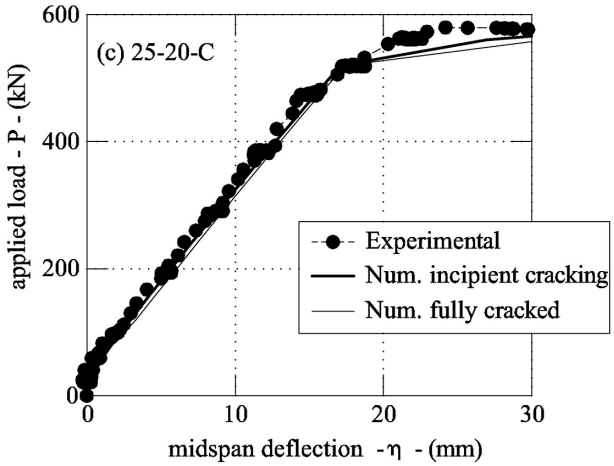

FIGURE 11 Comparison between the experimental data and the results of the three-stage model: (a) P–η curves of the beam 25-20-A; (b) P–η curves of the beam 25-20-B; (c) P–η curves of the beam 25-20-C

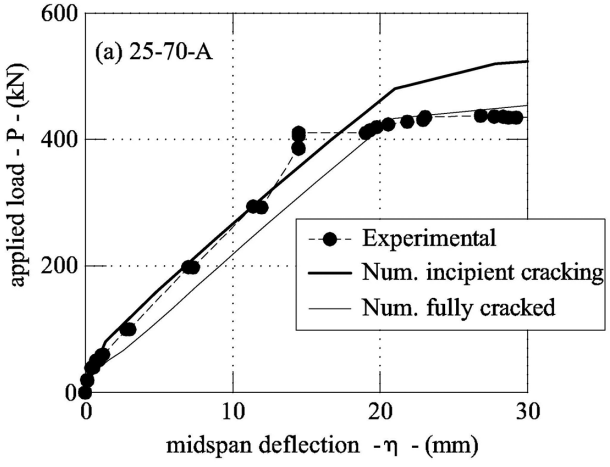

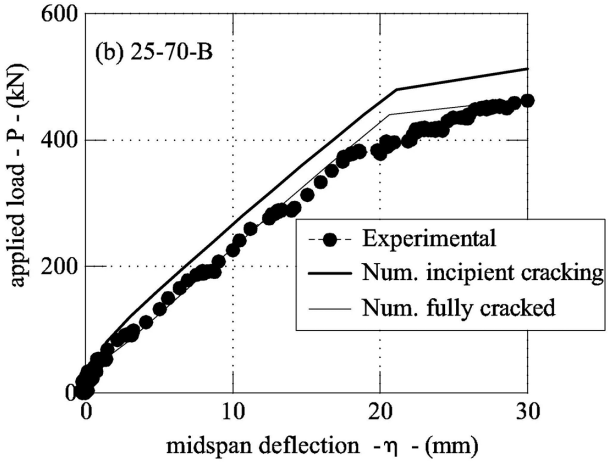

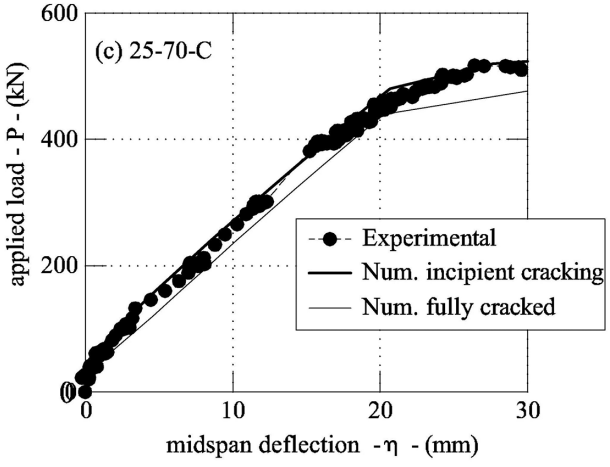

FIGURE 12 Comparison between the experimental data and the results of the three-stage model: (a) P–η curves of the beam 25-70-A; (b) P–η curves of the beam 25-70-B; (c) P–η curves of the beam 25-70-C

the type of fiber. Thus, when f_{R1} (corresponding to a crack width = 0.5 mm), f_{R2} (corresponding to a crack width = 1.5 mm), f_{R3} (corresponding to a crack width = 2.5 mm), and f_{R4} (corresponding to a crack width of 3.5 mm) are experimentally measured in accordance with EN14651,[17] the stress–strain relationship is computed in the same way[23] both for industrial manufactured steel fibers and RSF, without any distinction. In particular, the stress-cracks width law proposed

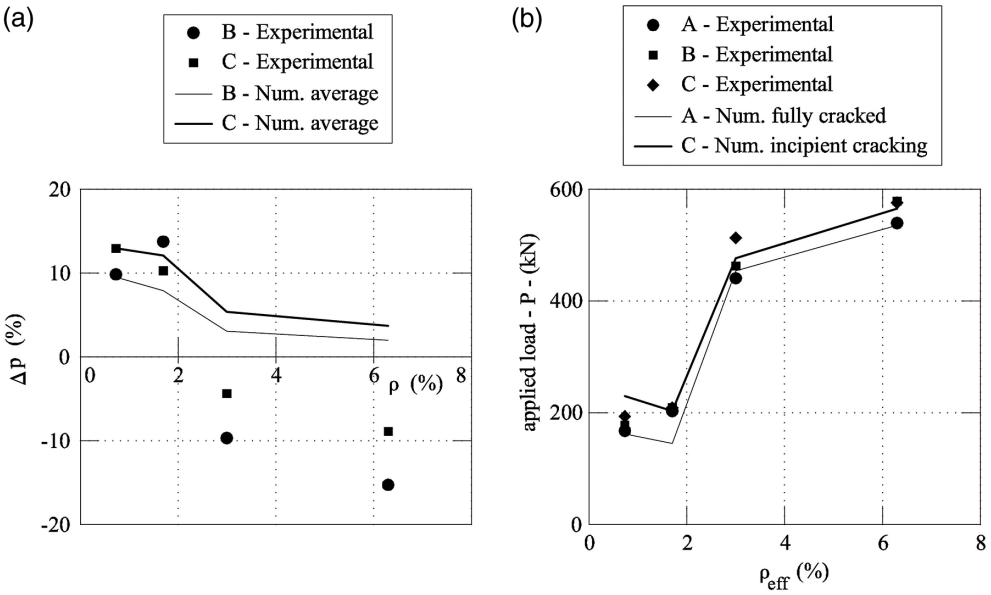

FIGURE 13 Comparison between the experimental and the results of the three-stage model: (a) increase in load Δp in concretes B e C as a function of the effective reinforcement ratio ρ_{eff}; (b) the load P at $\eta = 30$ mm

by Chiaia et al.[8] is adopted herein, whose parameters (i.e., f_{R1}, f_{R2}, f_{R3}, and f_{R4}) have been experimentally measured and reported in Table 2.

As a result, the three-stage model provides the P–η curves, which can be compared with those obtained in the tests (see Figure 2). This comparison is illustrated in Figure 9, Figure 10, Figure 11, and Figure 12 for the beams 12-20, 12-70, 25-20, and 25-70, respectively. In each figure, the range is calculated separately for the three types of the cement-based mixtures (i.e., A, B, and C of Table 2). In almost all the cross-sections and for all the types of concrete, the P–η curves experimentally measured fall within the range bordered by those computed with the three-stage model at incipient cracking (upper bound) and in fully cracked conditions (lower bound). The agreement between the experimental data and the numerical results reveals the great reliability of the proposed model, especially in the serviceability stage.

Moreover, if analyzed in-depth, the ranges of P–η also provide useful information for designing RC and R/FRC beams. Indeed, the amplitude of the range varies, depending on the effective ratio of reinforcement, and on the content of fibers. For a given cross-section (or a given effective reinforcement ratio), the area encompassed by the range tends to decrease with the fiber volume fraction (compare, for instance, the range of plain concrete in Figure 9a, with those of Figure 9b—where $V_f = 0.5\%$—and with Figure 9c—where $V_f = 1\%$). In such cases, the presence of fibers seems to mitigate the effects produced by the randomness of crack patterns in the tensile zone.

Similarly, for the same content of fibers, the amplitude of the range is reduced with the effective reinforcement ratio. For instance, in the P–η curves depicted in Figure 11 and related to beam 25-20 beams (with the highest ρ_{eff}), there are no significant differences between the situations of incipient cracking and fully cracked, especially in presence of fibers (see Figure 11b,c). Therefore, the effect produced by the fibers on the deflection of beams in bending is negligible in these cases.

Also, by comparing Figures 10 and 11, it would seem that the stiffening effect of fibers is less relevant for elements with higher cover. This effect, however, may be due, at least in part, to the simplification of the definition of the effective area. It seems that the effective area should also be limited to a maximum distance from the bar, probably depending upon the bar diameter. A more elaborate definition of the effective area, however, requires further research. Even so the cover does seem to have an effect since in all cases the experimental curve seems to be closer to the naked bar curve for the higher cover. This could be due to higher stresses in steel for the same load level.

Also, the marginal contribution of fibers in highly reinforced concrete beams can be deduced from Figure 13a, which shows the comparison between the experimental and theoretical values of Δp computed with Equation (1) when η is 1/500 of the span length (i.e., 7 mm in the beam of Figure 1a). More precisely, in the theoretical evaluation of Δp, $P_{R/FRC}$, and P_{RC} are assumed to be the average values of P taken, for a given η, on the two bounds of the P–η curves. In Figure 13a, the values of Δp provided by the three-stage model are close to those experimentally measured when the percentage of rebar in tension is lower than 2%. On the contrary, if $\rho > 3\%$, there is a dramatic reduction of Δp, even if the theoretical values remain positive and those

experimentally measured are negative. Indeed, in the three-stage model proposed herein, the interaction between cracks and the decrease in tension-stiffening are not considered.

Nevertheless, this phenomenon, concerning highly reinforced concrete beams, seems to occur only in the serviceability stage. After yielding of reinforcement, it vanishes, and the proposed model is able to predict the possible range of the loads acting on all the types of beams. As a matter of fact, in Figure 13b, almost all the experimental values fall within the theoretical range of P evaluated when $\eta = 30$ mm. In this figure, in order to maximize the amplitude of the range, the upper bound is obtained in R/FRC beams with the maximum percentage of fibers at incipient cracking, whereas the lower bound refers to fully cracked RC beams.

5 | CONCLUSIONS

The results of the experimental and theoretical investigations previously described can be summarized with the following points:

1. In the serviceability stage, the addition of fibers reduces the deflection of beams in bending, under the same load conditions. This reduction is particularly evident when the effective ratio of rebar in tension in lower than 2%;
2. For higher percentages, elements with fibers can exhibit larger deformations than members without fibers, probably due to the temporary closure of the existing cracks when new cracks appear;
3. When the yielding of rebars occurs, both the experimental and numerical analyses show higher external loads in R/FRC than in RC beams, having the same amount of rebar in tension and the same deflection;
4. In general, all the P–η curves experimentally evaluated are within a theoretical range, herein computed with a three-stage model, whose bounds correspond to the maximum (at incipient cracking) and minimum (fully cracked) tension-stiffening, respectively;
5. The amplitude of the range of the P–η curves tends to reduce as the percentage of rebar in tension increases. When $\rho_{\text{eff}} > 3\%$, for a given applied load, the presence of fibers does not modify the deflection (and the range between the behavior at the crack and the behavior at the section at mid-point between cracks becomes increasingly narrow);
6. By using the proposed three-stage model, the optimal combination of rebars and fibers (which could also be recycled) can be defined. For instance, when the mechanical properties of FRC are known, either the amount of rebar or the shape of the cross-section can be optimized, in order to minimize the deflections in service and maximize the bearing capacity at failure.

Finally, as the volume of concrete or the area of steel rebar can be reduced by the presence of recycled steel fibers, the proposed model can be used to design new concrete structures, having the same mechanical performances but a reduced carbon footprint. Thus, future research will be devoted to analyze both the mechanical and the environmental performance of concrete beams made with virgin and/or recycled materials.

ACKNOWLEDGMENTS

The experimental results presented in this this paper were obtained within the framework of the Research program *Uso de hormigones con fibras metálicas de NFU en estructuras integrales* lead by COMSA EMTE, S.A. with the participation of FHECOR Consulting Engineers and partially funded by *Centro de Desarrollo Tecnológico Industrial* (CDTI) an organism of the Spanish Ministry of Science and Technology, under project number IDI-20110480. The data that support the findings of this study are available on request from the corresponding author. The data are not publicly available due to privacy or ethical restrictions.

NOTATIONS

$A_{c,\text{eff}}$	effective cross-sectional area of concrete in tension
A_s	cross sectional area of reinforcement in tension
B	width of a beam cross-section
c	effective concrete cover
d	effective depth of a cross-section
f_c	compressive strength of concrete
f_{ct}	axial tensile strength of concrete
f_{R1}, f_{R2}, f_{R3}, f_{R4}	residual axial tensile strength of concrete defined in accordance with EN 14651[17]
H	depth of a beam cross-section
L	length of a beam in bending
M	bending moment
M_a, M_b	bending moment in virtual and real structures, respectively
N	axial force
P	applied concentrated load on real beam
p_s	perimeter of rebar
q	applied distributed load on real beam
s	slip between steel and concrete

s_r	crack spacing
U	applied concentrated load on virtual beam
w	crack width
y	vertical coordinate
z	horizontal coordinate
χ	cross-sectional curvature
χ_b	cross-sectional curvature in real beam
Δp	increment of applied load due to fiber-reinforcement
ε	strain
ε_c	strain in concrete or FRC
ε_s	strain in steel rebar
Φ	diameter of a reinforcing bar
η	deflection of a beam in bending
λ	strain in a cross-section at y 0
ρ	reinforcement ratio for longitudinal rebar in tension
σ	stress
σ_c	stress in concrete or FRC
σ_s	stress in steel rebar
τ	bond stress at the interface between steel and concrete

DATA AVAILABILITY STATEMENT

The data that support the findings of this study are available on request from the corresponding author. The data are not publicly available due to privacy or ethical restrictions.

ORCID

Alessandro P. Fantilli https://orcid.org/0000-0003-0383-7191
Benedetta Orfeo https://orcid.org/0000-0002-3061-7533
Alejandro Pérez Caldentey https://orcid.org/0000-0002-8575-1860

REFERENCES

1. International Federation for Structural Concrete. Model Code 2010—Final draft. Lausanne: *fib*; 2012 *fib* Bulletin 65-66.
2. American concrete Institute. ACI 314R-16: guide to simplified Design for Reinforced Concrete Buildings. Farmington Hills, MI: ACI; 2016.
3. Caldentey AP, Cembranos JM, Peiretti HC. Slenderness limits for deflection control: a new formulation for flexural reinforced concrete elements. Struct Concr. 2017;18:118–27. https://doi.org/10.1002/suco.201600062.
4. International Federation for Structural Concrete. Serviceability limit state of concrete structures. Lausanne: *fib*; 2019 fib Bulletin 92.
5. Fantilli AP, Ferretti D, Iori I, Vallini P. Flexural deformability of reinforced concrete beams. ASCE J Struct Eng. 1998;124(9):1041–9.
6. Fantilli AP, Vallini P. Tension stiffening range in FRC elements. 6th RILEM Symposium on Fibre Reinforced Concrete FRC—BEFIB 2004. Varenna, Italy: RILEM Publications SARL; 2004.
7. Cheng C, Cai H, Li J, Zhong P, Huang B, Sui L, et al. One-dimensional extended FEM based approach for predicting the tensile behavior of SHCC-FRP composites. Eng Fract Mech. 2020;225:106775.
8. Chiaia B, Fantilli AP, Vallini P. Evaluation of crack width in FRC structures and application to tunnel linings. Mater Struct. 2009;42(3):339–51.
9. Vasanelli E, Micelli F, Aiello MA, Plizzari G. Long term behavior of FRC flexural beams under sustained load. Eng Struct. 2013;56:1858–67.
10. Hamrat M, Boulekbache B, Tahenni T, Chemrouk M, Amziane S. Experimental study of deflection of steel fibre reinforced concrete beams: comparison of different design codes. Eur J Environ Civil Eng. 2020. https://doi.org/10.1080/19648189.2020.1749941.
11. Ashour SA, Mahmood KM, Wafa FF. Service load deflections of high-strength fiber reinforced concrete beams. J King Saud Univ—Eng Sci. 2000;12(2):21–46.
12. Domski J, Zakrzewski M. Deflection of steel fiber reinforced concrete beams based on waste sand. MDPI Mater. 2020;13:392–417.
13. Perez Caldentey A, Mestre Garcia C, Mendoza Cembranos J. A new way to sustainability: designing more slender building structures by using recycled steel fibers. Zadar, Croatia: Proceedings of the 1st International Conference on Construction Materials for Sustainable Future; 2017.p. 19–21.
14. Groli G. Crack width control in RC elements with recycled steel fibres and applications to integral structures: theoretical and experimental study. PhD Thesis, E.T.S.I. Caminos, Canales y Puertos. Technical University of Madrid (UPM); 2014.
15. Groli G, Pérez Caldentey A, Soto AG. Cracking performance of SCC reinforced with recycled fibres—an experimental study. Struct Concr. 2014;15:136–53. https://doi.org/10.1002/suco.201300008.
16. Pérez Caldentey A, Corres Peiretti H, Peset Iribarren J, Giraldo Soto A. Cracking of RC members revisited: influence of cover, ϕ/ρs, ef and stirrup spacing—an experimental and theoretical study. Struct Concr. 2013;14:69–78. https://doi.org/10.1002/suco.201200016.
17. European Standard. EN 14651: test method for metallic fibered concrete—measuring the flexural tensile strength (limit of proportionality (LOP), residual). London, England: CEN; 2005.
18. European Standard. EN 1992-1-1: Eurocode 2: design of concrete structures—part 1–1: general rules and rules for buildings. Brussels, Belgium: CEN; 2004.
19. Fantilli AP, Vallini P. Strains in steel bars of reinforced concrete elements subjected to repeated loads. J Strain Anal Eng Des. 2004;39(5):447–57.
20. Fantilli AP, Tondolo F. Residual crack width in RC and R/FRC ties subjected to repeated loads. 3rd FRC international workshop on fibre reinforced concrete: from design to structural applications. Italia: Desenzano; 2018. p. 28–30.
21. Clark AP. Cracking in reinforced concrete flexural members. J Am Concr Inst. 1956;27(8):851–62.
22. Cheng C, Cheng L. Single crack-based model for FRP shear-strengthened RC beams. J Compos Construct. 2019;23-4. https://doi.org/10.1061/(ASCE)CC.1943-5614.0000953.
23. Rilem TC. 162 TDF. σ-ε-design method. Final recommendation. Mater Struct. 2003;36:560–7.

AUTHOR BIOGRAPHIES

Alessandro P. Fantilli, Associate Professor, Department of Structural, Building and Geotechnical Engineering, Politecnico di Torino, Corso Duca degli Abruzzi 24, 10129 Torino, Italy.
Email: alessandro.fantilli@polito.it

Benedetta Orfeo, PhD Student, Department of Continuum Mechanics and Structures, Universidad Politécnica de Madrid, Calle del Prof. Aranguren, 3, 28040, Madrid, Spain.
Email: benedetta.orfeo@alumnos.upm.es

Alejandro Pérez Caldentey, Associate Professor, Department of Mechanics of Continuous Media and Theory of Structures, Technical University of Madrid & FHECOR Consulting Engineers, Prof. Aranguren, 3, 28040, Madrid, Spain.
Email: apc@fhecor.es

How to cite this article: Fantilli AP, Orfeo B, Pérez Caldentey A. The deflection of reinforced concrete beams containing recycled steel fibers. *Structural Concrete*. 2021;22:2089–2104. https://doi.org/10.1002/suco.202000729